# Self-Organized Tubular Structures as Platforms for Quantum Dots

Rabih Makki,[†] Xin Ji, Hedi Mattoussi, and Oliver Steinbock*

Florida State University Department of Chemistry and Biochemistry, Tallahassee, Florida 32306-4390, United States

S *Supporting Information*

ABSTRACT: The combination of top-down and bottom-up approaches offers great opportunities for the production of complex materials and devices. We demonstrate this approach by incorporating luminescent CdSe-ZnS nanoparticles into macroscopic tube structures that form as the result of externally controlled self-organization. The 1−2 mm wide hollow tubes consist of silica-supported zinc oxide/hydroxide and are formed by controlled injection of aqueous zinc sulfate into a sodium silicate solution. The primary growth region at the top of the tube is pinned to a robotic arm that moves upward at constant speed. Dispersed within the injected zinc solution are 3.4 nm CdSe-ZnS quantum dots (QDs) capped by DHLA-PEG−OCH$_3$ ligands. Fluorescence measurements of the washed and dried tubes reveal the presence of trapped QDs at an estimated number density of 10^{10} QDs per millimeter of tube length. The successful inclusion of the nanoparticles is further supported by electron microscopy and energy dispersive X-ray spectroscopy, with the latter suggesting a nearly homogeneous QD distribution across the tube wall. Exposure of the samples to copper sulfate solution induces quenching of about 90% of the tubes' fluorescence intensity. This quenching shows that the large majority of the QDs is chemically accessible within the microporous, about 15-μm-wide tube wall. We suggest possible applications of such QD-hosting tube systems as convenient sensors in microfluidic and related applications.
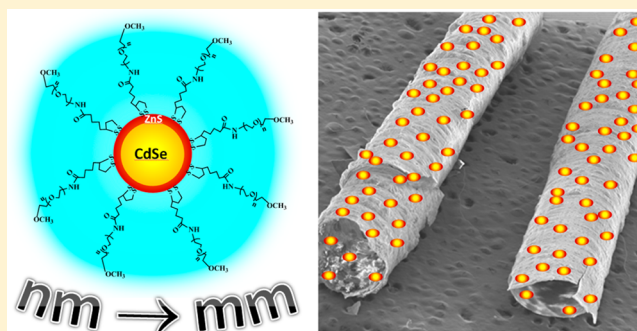
1. INTRODUCTION

The production of materials and devices under nonequilibrium conditions is a widely unexplored area of chemistry but holds great potential for bridging the complexity gap between biological and synthetic materials.[1−3] The rational development of this novel type of materials science requires the study of carefully chosen model systems and the theoretical analysis of the underlying physicochemical principles. A basic but powerful example is the creation of a solid within two opposing concentration gradients that allow the control of the product's size, position, and chemical composition. To carry out this process, the gradients must be sufficiently steep and stable, which implies that appropriate driving forces are needed. Self-organizing reaction-diffusion systems, such as the Belousov−Zhabotinsky reaction and the chlorite−iodide−malonic acid reaction,[4−6] can accomplish this task because of nonlinearities in their reaction mechanisms. However, these systems typically do not create solid materials or have other shortcomings, and hence, to date, materials science has no means of utilizing these powerful forms of chemical self-organization far from thermodynamic equilibrium.

A promising stepping stone along this ambitious path are tubular precipitation structures created in reaction-diffusion-advection processes from compounds such as silicate, carbonate, borate and inorganic anions.[7−13] This class of reactions, which is closely related to the well-known silica-garden demonstration, is an ideal model system for studying the nonequilibrium synthesis of materials.[14] The hollow tubes have diameters of a few micrometers up to several millimeters and their thin wall forms in response to self-maintained, opposing concentration gradients of the reactants.[15,16] The wall typically consists of an outer layer rich in silica or a similar anion-derived substance, whereas the inner surface is rich in metal hydroxides or oxides.[17,18] Several other modifications have been reported in the recent literature that also include tubules involving materials such as iron sulfide, iron oxides, calcium carbonate, aluminosilicates, and polyoxometalates.[19−23] Accordingly some of these tube materials can be powerful catalysts.[24] Other studies reported luminescent and super-paramagnetic behavior for the cases of silica/ZnO and silica/magnetite tubes, respectively.[25,26]

In the simplest case, the tube systems can be produced from small seed crystals, polycrystalline pellets, or reactant-loaded polymer beads. Thouvenel-Romans et al. described a modification in which one of the two reactant solutions is injected (typically at a constant rate and in vertical direction) into a large volume of the other reactant.[27,28] Their approach usually yields a single tube that nucleates at the injection nozzle and then extends its length by fast precipitation reactions at its other orifice. This growth process is accompanied by a slower, less striking secondary growth that slowly increases the wall thickness.[29] In the case of jetting growth, during which the orifices are never capped, the increase in tube length occurs at a
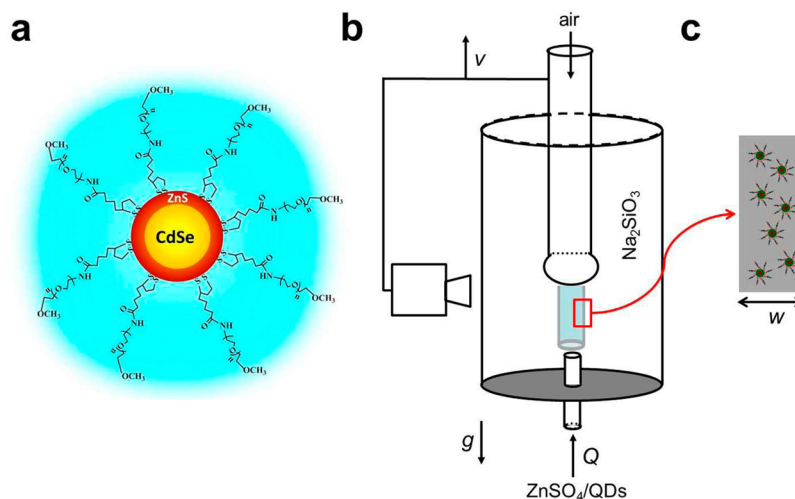
Figure 1. (a) Schematic drawing of CdSe-ZnS QD capped by DHLA-PEG−OCH$_3$ ligands (PEG 750, n = 15). The QD radius is 3.4 nm. (b) Schematic representation of the experimental setup. A computer-controlled motor moves an air-filled glass rod and a video camera upward at a constant speed of v = 2 mm/s. Attached to the bottom end of the glass rod is a large gas bubble. Simultaneously, ZnSO$_4$/QDs colloidal solution is injected at a constant pump rate (Q = 10 mL/h) into a large reservoir of silicate solution. The vector g denotes gravity. (c) Schematic drawing showing a close-up view of a tube wall (thickness w) with incorporated QDs.

constant speed and is the result of opposing gradients in the concentrations of the precipitating metal ion, the polymerizing silicate, and the pH. Notice that these steep gradients are stationary in the comoving system of the expanding tube and, hence, fulfill the requirements laid out in our opening statement. Accordingly, the wall material is created under stationary, nonequilibrium conditions that under most other circumstances would swiftly dissipate.

The primary goal of this article is to demonstrate that this unconventional synthesis method can be combined with modern approaches that attract vigorous attention in the field of nanotechnology.[30−32] We will specifically show that the self-organized tubular precipitation structures can be used as a platform for the spontaneous incorporation of semiconductor nanocrystals (quantum dots, QDs) and that this incorporation can be carried out during the growth of the macroscopic structure. QDs along with a whole array of nanostructured materials made of metals, metal oxides, and metal chalcogeneides exhibit unique chemical and photophysical properties that are controlled by size or composition or both.[30] These materials often exhibit properties that are not observed either at the molecular scale or for their bulk parent materials. For instance, QDs exhibit size-tunable broad absorption and narrow emission spectra, along with redox active properties.[30,31] They can engage in efficient energy transfer or charge transfer interactions with proximal dyes or redox active molecules.[32] Indeed, luminescent QDs have been used in designing a variety of sensing assemblies based on both energy transfer and electron transfer processes.[31,32] In this respect, the present study is also linked to recent work on the integration of such materials in various complex structures, ranging from QDs embedded in heterostructure films for photovoltaic and light emitting devices to integration within biological constructs for cellular imaging and fluorescence sensing.[33−35] Integration of these nanomaterials into self-organized tubular precipitates hence offers intriguing possibilities regarding sensor-application in microfluidic systems, the passivation of QDs as well as optoelectronic and photovoltaic applications.[31,32,36−39]

2. EXPERIMENTAL SECTION

2.1. Materials. The reagents used in this work are zinc sulfate heptahydrate (ZnSO$_4$·7H$_2$O, Fisher), sodium metasilicate pentahydrate (Na$_2$SiO$_3$·5H$_2$O, Fisher), sodium hydroxide (NaOH, Fluka), and QDs (see below). All chemicals are of analytical grade and solutions are prepared using ultrapure water (18 MΩ cm; Easy-pure UV, Barnstead).

2.2. Quantum Dot Synthesis. The quantum dots used in the present study are made of CdSe-ZnS core−shell nanocrystals with a first absorption (band edge) peak at 553 nm and a photoluminescence (PL) emission maximum at 578 nm. These nanocrystals are prepared in two successive reaction steps.[40,41] The CdSe core are first grown via reduction of cadmium and selenium precursors at high temperature in a hot (300−350 °C) coordinating solvent. This solvent is a mixture made of trioctyl phosphine (TOP), trioctyl phosphine oxide (TOPO), and alkylamines. The CdSe core is overcoated with ∼6 monolayers of ZnS using zinc and sulfur precursors.[40−42] The overcoating procedure is also carried out using coordinating solvent mixture, but at lower temperature (150−180 °C). The average nanocrystal size (core plus shell) extracted from a combination correlating the first absorption peak, TEM, and small-angle X-ray scattering is 3.4 nm in radius.[42,43] The hydrophobic QDs (TOP/TOPO-capped) are rendered hydrophilic via ligand exchange using dihydrolipoic acid appended with poly(ethylene glycol) (DHLA-PEG), as described in previous reports.[44]

We chose these CdSe-ZnS core−shell nanocrystals for the present study because they exhibit high photoluminescence quantum yields and a great resistance to photo- and chemical degradation, compared to say core only nanocrystals. In addition, the use of DHLA-PEG ligands to transfer the nanocrystals to water media is beneficial for our present system, as these provide QDs with long-term stability in acidic and basic conditions. DHLA-PEG-QDs also exhibit great colloidal stability in the presence of added salts along with reduced nonspecific interactions. The stability to pH changes and in the presence of added salts and reducing agents, in

particular, is important as the tubular growth is carried under basic conditions and in the presence of excess counterions.

2.3. Tube Formation. As shown in Figure 1, QD-doped silica tubes are prepared by the hydrodynamic injection of an aqueous solution containing $ZnSO_4$ (0.50 M) and the dispersed QDs into a large reservoir (approximately 60 mL) of sodium silicate solution (1.0 M) at (22 ± 1) °C. The QD concentration in the injected solution is 0.24 μM unless otherwise noted. A glass capillary (length = 27 mm, inner diameter = 1.1 mm) is used to deliver the zinc/QD solution into a cylindrical glass vessel (height ≈ 90 mm, inner diameter = 32 mm) containing the silicate solution. The flow rate of the injected solution is controlled by a syringe pump (KD Scientific 200) and kept constant at 10 mL/h. Once the injected solution leaves the upper end of the glass capillary, a single tube starts to grow. Instantly, the growing tube is pinned to an air bubble which is created using an air-filled syringe and held at the lower end of a hollow glass tube. The latter (length = 24 cm, inner diameter = 4.0 mm) is centered in the middle of the glass cylinder and positioned 3−5 mm above the glass capillary. After pinning is achieved, the glass tube moves up vertically at a constant, predetermined speed of 2 mm/s. A charge-coupled device camera (CCD, COHU 2122) is mechanically connected to the glass rod and both components move together in the vertical direction. The motion is generated by a servo motor/controller system (BLM-N23-50-1000-B, CDS-3310, Galil). Using this setup, we can select the vertical growth velocity of the tube as the speed of pinning glass rod. The camera signal is digitized at a typical rate of 4 frames/s by a frame grabber board (DT 3155, Data Translation) and HL Image ++97 software. More details concerning the experimental setup can be found in ref 45. For further characterization, we remove the structures from the silicate solution. Then they are washed three to four times with water and dried overnight at ambient conditions.

2.4. Characterization. We record scanning electron microscopy (SEM) images on a JEOL JSM-5900 scanning electron microscope coupled with an energy dispersive X-ray spectrometer (EDS) at an acceleration voltage of typically 30 kV. Transmission electron microscopy (TEM) is performed on a JEOL 2010 instrument operating at 200 kV. The fluorescence spectra are collected on a Fluorolog-3 spectrometer (HORIBA Jobin Yvon Inc., Edison, NJ) using an excitation wavelength of 350 nm. Both the excitation and emission slit widths are 3 nm. The instrument is equipped with a fast TBX PMT detector and an air cooled CCD camera.

3. RESULTS

In a recent report, we have shown that the growth zone for similarly prepared copper hydroxide-silica tubes is located either at the air bubble or at the tube's base (i.e., close to the solution-delivering glass capillary). This behavior depends on the velocity of the glass rod and the flow rate of the injected solution. In this study, we fixed these experimental parameters at values that ensure vertical growth at the air bubble only.[45] Figure 2 shows two snapshots from a representative experiment where image frame (b) is recorded 2 s after frame (a). Notice that our image data (Figure 2) are recorded using a moving video camera that travels along with the glass rod and pinning bubble in an upward direction. The primary wall growth occurs at the reactive interface right underneath the bubble and generates a fairly straight, vertical tube. The radius of the tube is nearly constant (r_{exp} = 0.66 mm) and very close to the one
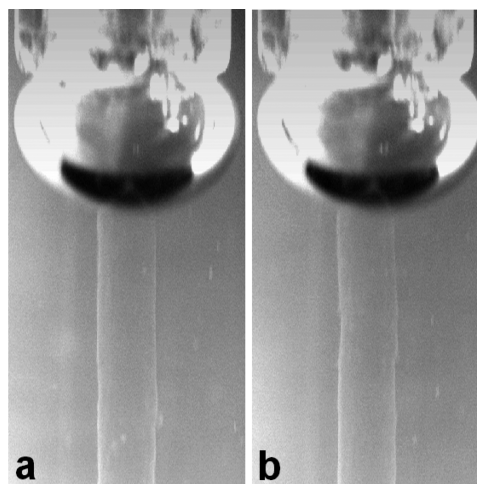

Figure 2. Tube formation imaged by a comoving video camera. The large ellipsoidal-like feature in the upper half of the images is the gas bubble that pins the leading reaction zone of the tube and also acts as a cushion to the upward moving glass tube. Time interval between the two snapshots is 2 s. Field of view: 3.9×7.8 mm^2.

expected[45] from volume conservation of the injected solution (r_{cal} = 0.665 mm).

Figure 3a shows the emission spectra for a tube formed by the injection of only $ZnSO_4$ solution (no CdSe-ZnS nanocrystals, black curve) and a tube formed by the injection of $ZnSO_4$ solution with dispersed CdSe-ZnS nanocrystals (red curve). In both cases, the formed tubes were removed from the sodium silicate solution, washed 3−4 times with water, and then left to dry under ambient conditions. Measurements were performed on the dried tubes using an excitation wavelength of 350 nm. Both tubes generate photoemission with a peak at 375 nm, which corresponds to the fluorescence of ZnO crystals. The red curve shows an additional peak at 578 nm which is characteristic of the CdSe-ZnS nanocrystals (see the inset of Figure 3a). This result indicates the successful incorporation of CdSe-ZnS QDs into the wall of the tube formed by the injection of $ZnSO_4$ solution containing dispersed CdSe-ZnS nanocrystals. The net effect of the QDs is further illustrated by the spectra shown in the inset of Figure 3a. The blue curve is obtained by subtracting the fluorescence intensity of the black curve from that of the red one. The green curve represents the emission spectrum of a reference sample containing pure QD suspension ([QD] = 0.24 μM). The absence of a discernible change (shift or broadening) in the fluorescence properties of the incorporated QDs indicates the absence of strong chemical interactions between the QDs and the surrounding silica or metal oxide/hydroxide matrix. We, therefore, assume that the QDs are individually, physically trapped inside the microporous tube wall.

In additional experiments, we evaluated the extent of the QD inclusion and specifically ruled out the possibility that the nanoparticles are only loosely attached to the surface of the tube wall. For these experiments, the tubes are removed from the silicate solution, gently rinsed three or four times with water and subsequently kept in water for 1 to 7 days. The resulting samples are then dried and analyzed by fluorescence measurements. The corresponding intensity values (see Supporting Information Figure S1) show no systematic decrease over time. Consequently, the QDs are firmly immobilized within (or on) the tube material and do not easily leach out into the
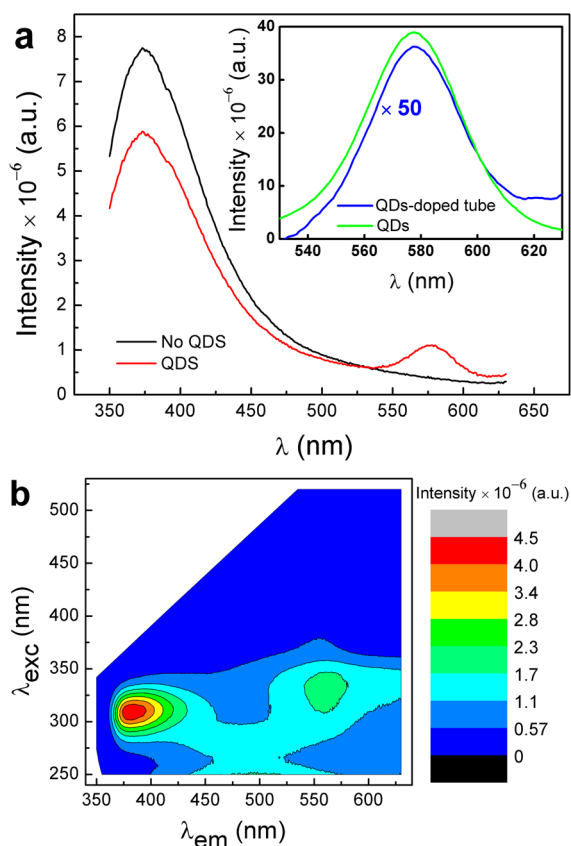
Figure 3. (a) Emission spectra of a tube formed by the injection of only $ZnSO_4$ solution (no CdSe-ZnS nanocrystals, black curve) and a tube formed by the injection of $ZnSO_4$ solution with dispersed CdSe-ZnS nanocrystals (red curve). The inset shows the emission spectra for QDs in different environments. The blue curve shows the contribution of the QDs trapped inside a tube wall and is obtained by subtracting the fluorescence intensity of the black curve from that of the red one. The green line represents the emission spectrum of a reference sample containing containing only dispersed QDs ([QD] = 0.24 μM). The intensity of the blue line is multiplied by 50 to enhance the signal. Excitation wavelength: λ_{exc} = 350 nm. (b) 2D fluorescence excitation spectrum of a typical QD-containing tube.

surrounding solution. Further details are shown in the 2D fluorescence excitation spectrum of a typical QD-hosting tube (Figure 3b). The spectrum is obtained by measuring the fluorescence emission via scanning both the excitation wavelength and the emission wavelength. The contour plot reveals that QD emission is optimal for excitation wavelengths in the range of 300−350 nm. Transmission electron microscopy provides additional evidence for the incorporation into the walls of the formed tubes. Figure 4 is a representative TEM image of a tube fragment showing nanoparticles with a mean diameter that matches the value expected for our QDs (see Experimental Section).

To gain more insights into the macroscopic morphology and surface texture of the QD-containing precipitation structures, we imaged numerous samples using scanning electron microscopy. Figure 5a shows two tubes that extend with a uniform radius. Figure 5b shows the cross-section of a typical tube. It supports our conclusion that the tubes are hollow and remain hollow after drying. The inner surface appears more rugged than the outer one. Figure 5c shows the thickness of a tube wall, in which the inner (outer) surface extends in the left (right) edge of the frame. Clearly, the tube wall is not
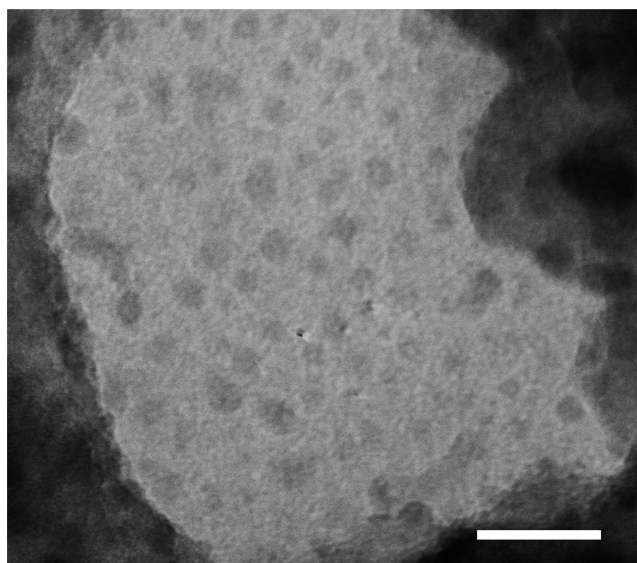

Figure 4. TEM of a tube fragment showing particles with a mean diameter that matches the value expected for the injected QDs. Scale bar: 20 nm.
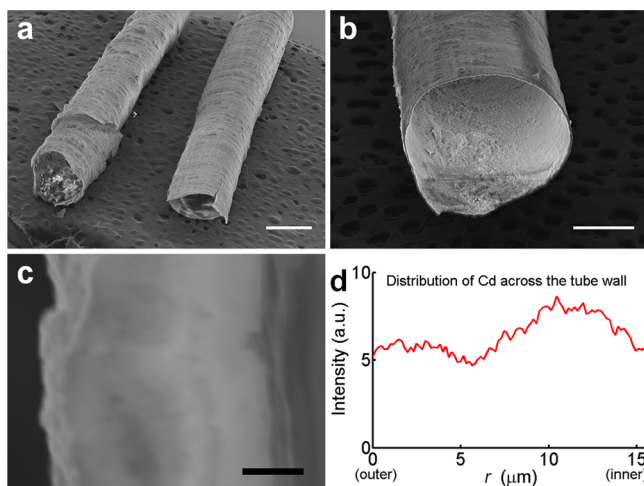

Figure 5. (a−c) SEM micrographs of QD-containing tubes showing the surface morphology of the outer (a) and inner tube wall (b). The cross-section of a typical tube wall is shown in (c). Here, the exterior (interior) surface of the tube extends close to the left (right) image border. (d) Distribution of cadmium across the tube wall as obtained from the EDS map of the area shown in (c). The r-values of 0 and 15 μm correspond to the approximate positions of the outer and inner surface, respectively. Scale bars: 1 mm (a), 500 μm (b), 5 μm (c). QD concentration in the injected solution is 0.1 μM in (b) and 0.24 μM otherwise.

homogeneous. Figure 5d shows the corresponding EDS map of the distribution of cadmium across the tube wall. The abscissa denotes the radial space coordinate across the tube wall with 0 and 15 μm marking the positions of the outer and inner wall surface, respectively. The ordinate represents the EDS intensities averaged in the perpendicular direction. The data reveal a nearly uniform distribution of QDs across the exterior silica-rich and interior zinc oxide/hydroxide layers and possibly slightly elevated QD concentrations within the interior half of the wall. The wall-spanning presence of the QDs is surprising because they are suspended only in the injected, interior solution but not in the surrounding reservoir. A possible

explanation of this finding is related to a recent study reporting that the very slow thickening of the tube wall is strictly inward directed.[29] Although the latter study did not include QDs, this unidirectional radial growth would allow for the continuous incorporation of QDs into the widening wall.

To measure the chemical accessibility of the trapped QDs, we investigated the fluorescence quenching of the QDs-doped tubes by copper ions. Changes in QD fluorescence when exposed to soluble ions such as Cu^{2+} and Pb^{2+} have been explored by several groups in the past decade.[46−48] For instance Rosenzweig et al. showed that thioglycerol-capped CdS QDs exhibit specific interactions with copper ions, and measured a fluorescence quenching commensurate with the ion concentration in the medium; a detection threshold of 0.1 μM was reported for that system.[46] Similarly, Xie et al. reported that CdSe-ZnS QDs capped with bovine serum albumin were readily quenched by soluble copper ions.[47] In the latter example, the authors proposed a metal ion exchange between the soluble copper ions and the QD surface, altering the rate of radiative recombination of the electron−hole pair (exciton) and producing concentration-dependent quenching in the QD emission.

Figure 6 shows the time-dependent fluorescence intensity ratio, I/I_0, measured during representative quenching experi-
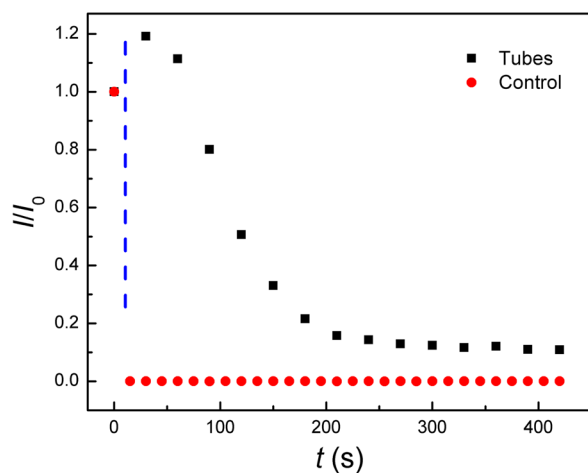

Figure 6. Time-intensity plots showing fluorescence quenching by the introduction of copper ion. Black squares represent the relative fluorescence intensity of a prepared tube (tube length = 1.3 cm) and red circles denote the relative fluorescence intensity of a reference sample containing 300−400 μL of a colloidal suspension of QDs ([QDs] = 0.24 μM). I represents the fluorescence intensity at time t and I_0 represents the fluorescence intensity at t = 0. The dashed blue line denotes the time at which a copper sulfate solution ([$CuSO_4$] = 0.1 M, 300−400 μL) is added. Excitation and emission wavelengths: λ_{exc} = 350 nm; λ_{em} = 578 nm.

ments where I_0 denotes the initial intensity prior to quenching (t = 0). The Figure shows two data sets obtained for (i) a carefully washed tube (tube length = 1.3 cm, black squares) and (ii) a reference sample containing 300−400 μL of a colloidal suspension of QDs ([QD] = 0.24 μM, red circles). The dashed blue line denotes the time at which copper sulfate solution ([$CuSO_4$] = 0.1 M, 300−400 μL) is added. We note that the tube was initially soaked in 300−400 μL of water to eliminate undesired artifacts that might result from wetting the tube surface. The addition of copper sulfate solution causes the relative fluorescence intensity of the reference solution to drop

very rapidly from 1 to 0, indicating fluorescence quenching of all the QDs. However, in the case of the tube sample, the relative fluorescence intensity gradually drops and saturates at 0.1 within approximately 200 s. Notice that the concentration of the added copper sulfate solution is much higher than the one required to quench the fluorescence of all QDs in the tube (micromolar range). Therefore, the observed nonzero saturation value is not caused by copper ion being a limiting reagent. The magnitude of the intensity drop indicates that around 90% of the trapped QDs are chemically accessible while the remaining 10% of the QDs are not accessible. We attribute the small increase in the fluorescence intensity upon the addition of copper sulfate to variations in the QDs' chemical environment as well as slight changes in the tube position.

Notice that the observed time required to quench the fluorescence of the accessible QDs (200 s) is surprisingly long for the thin walls of these tubular samples. If we consider the diffusion constant of Cu^{2+} ions in dilute aqueous solution (D = 0.7×10^{-5} cm^2 s^{-1}) and a typical wall thickness w = 15 μm, we find a diffusion time $t_d = w^2/(2D)$ of only 160 ms, which is 3 orders of magnitude smaller than the measured quenching time. Even if we assume that the hydrated wall is ten times thicker than the given value which is obtained from dry samples, there remains a significant difference in time scales. Accordingly Cu^{2+} motion within the hydrated wall must have a markedly smaller diffusion coefficient than that for dissolved copper ion in aqueous solution. A contributing factor might be that the inorganic wall structure is most likely charged. This conclusion was also reached by an electrochemical study of precipitated $BaSO_4$ membranes, which showed overall low permittivities for H^+ and much higher ones for hydroxide ion.[49]

Finally, we estimate the number of QDs trapped per unit length of tube. These measurements are based on a fluorometric method, which can yield only estimates because the fluorescence intensity varies strongly with the chemical environment of the QDs. In our measurements, tubes of different lengths are dissolved in 2 mL of hot sodium hydroxide solution (1.0 M). Fluorescence measurements of the obtained solutions are then performed using an excitation wavelength of 350 nm. In addition, we record a calibration curve (see Supporting Information Figure S2) for pure QD suspensions and otherwise similar conditions. For each tube solution, the concentration of the QDs is then deduced from the calibration curve to yield the number of QDs per unit length. The results indicate an average of $N = (1.5 \pm 0.8) \times 10^{10}$ particles/mm of tube length which is equivalent to 0.025 pmol/mm. The latter value allows us to estimate the volume fraction of QDs in the tube wall. For this, we assume that the core/shell QDs have a perfect spherical shape, a combined core−shell radius of r = 3.4 nm, and that the tube wall has a cross-sectional area of $A = w\pi d$, where d is the average tube diameter (here, 1.32 mm) and w denotes the average wall thickness (here, 15 μm). Accordingly, we find that about 0.004% of the tube wall volume is occupied by QDs. In addition, we find from the values of N and A that the concentration of QDs in the tube wall is (0.4 ± 0.2) μM. The latter concentration range compares remarkably well with the starting concentration of the QDs in the injected solution (0.24 μM). Considering the high solubility of the nanoparticles in aqueous solution and the rapid character of the precipitation reaction, we consider a reaction-induced enhancement of the QD concentration unlikely. Nonetheless, a certain increase might result from the drying of the initially hydrated and swollen tube structure.

4. CONCLUSION

In summary, we have demonstrated the incorporation of QDs into the walls of macroscopic silica-zinc oxide/hydroxide tubes *in situ* during the growth of the tube. Our approach combines recent advances in the field of nonequilibrium synthesis with modern semiconducting nanomaterials and brings together a range of unique features that span from controlled macroscopic shapes to high extinction coefficients and plasmonics. Our study also establishes that the trapped QDs are chemically accessible, which should make the tubular structures excellent devices for chemical sensing in microfluidic applications.

Moreover, our results open up new avenues for the study of self-organized solids with tailored physical and chemical features at the nano and microscale. For instance, it seems likely that the trapping of soft structures such as polymeric microbeads, bacteria, and viruses could be used to achieve tailored macroporosities in these materials. Notice that the possibility of postsynthetic processing was recently demonstrated by Roszol et al., who showed that Cu(OH)$_2$/silica tubes can be converted at high temperatures to CuO and Cu$_2$O silica tubes without compromising their macroscopic shape.[50] Additional possibilities include the incorporation of other nanoparticles (including metallic ones) and even the *in situ* production of the particles in the forming tube wall.

More work is also needed to explore how organic molecules and nanoparticles alter and control the macroscopic tube forming process. Such a feedback is conceivable but has not been demonstrated yet. Nonetheless, the tubes produced for this study show some unusual surface texture that ranges from closely spaced rings to network-like structures (see Figures 5a,b). Ring-like patterns are often present on the exterior surface of precipitation tubes, but their spacing in the presence of QDs is much shorter than expected. Additional work is needed to elucidate such possible dependence and explore whether more extreme cases can be induced. Of particular interest in this context would be to identify additives that can induce tube branching and other morphological transitions.

We suggest that our approach can be further applied to other nonequilibrium structures such as the inorganic microcones described in a recent study by the Aizenberg group[51] or silica biomorphs,[52,53] which includes a variety of leave-like and helical shapes. In addition, it is known that such nontrivial structures are not specific to a particular reaction or class of compounds but rather a universal feature of a wide range of rapid solidification processes.[54−56] Accordingly, we see ample opportunities for combining the physicochemical features of the self-organized macroscopic host structure and the nanoscopic guest units. If this methodology is as versatile as currently perceived, applications could also include the environmentally induced release of particles and molecules from custom-shaped objects.

ASSOCIATED CONTENT

Ⓢ Supporting Information

Results of leaching experiments, calibration curve (PDF). This material is available free of charge via the Internet at http://pubs.acs.org.

AUTHOR INFORMATION

Corresponding Author

steinbck@chem.fsu.edu.

Present Address

†Harvard University, Department of Earth and Planetary Sciences, Cambridge, Massachusetts 02142-1204, United States.

Notes

The authors declare no competing financial interest.

ACKNOWLEDGMENTS

REFERENCES

(1) Warren, S. C.; Guney-Altay, O.; Grzybowsky, B. A. *J. Phys. Chem. Lett.* **2012**, *3*, 2103−2111.
(2) Chekanov, Y. A.; Pojman, J. A. *J. Appl. Polym. Sci.* **2000**, *78*, 2398−2404.
(3) Suryanarayana, C. *Non-equilibrium Processing of Materials Pergamon Materials Series*; Cahn, R. W., Ed.; Elsevier Science: Oxford, 1999.
(4) Epstein, I. R.; Pojman, J. A. *An Introduction to Nonlinear Chemical Dynamics: Oscillations, Waves, Patterns, Chaos*; Oxford University Press: New York, 1998.
(5) Bánsági, T.; Steinbock, O. *Phys. Rev. Lett.* **2006**, *97*, 198301.
(6) De Kepper, P.; Castets, V.; Dulos, E.; Boissonade, J. *Physica D* **1991**, *49*, 161−169.
(7) Coatman, R. D.; Thomas, N. L.; Double, D. D. *J. Mater. Sci.* **1980**, *15*, 2017−2026.
(8) Cartwright, J. H. E.; García-Ruiz, J. M.; Novella, M. L.; Otálora, F. *J. Colloid Interface Sci.* **2002**, *256*, 351−359.
(9) Maselko, J.; Borisova, P.; Carnahan, M.; Dreyer, E.; Devon, R.; Schmoll, M.; Douthat, D. *J. Mater. Sci.* **2005**, *40*, 4671−4673.
(10) Panataleone, J.; Toth, A.; Horvath, D.; RoseFigura, L.; Morgan, W.; Maselko, J. *Phys. Rev. E* **2009**, *79*, 056221.
(11) Barge, L. M.; Doloboff, I. J.; White, L. M.; Stucky, G. D.; Russell, M. J.; Kanik, I. *Langmuir* **2012**, *28*, 3714−3721.
(12) Cartwright, J. H. E.; Escribano, B.; Khoklov, S.; Sainz-Diaz, C. I. *Phys. Chem. Chem. Phys.* **2011**, *13*, 1030−1036.
(13) Pratama, F. S.; Robinson, H. F.; Pagano, J. J. *Colloids Surf., A* **2011**, *389*, 127−133.
(14) Cooper, G. J. T.; Bowman, R. W.; Magennis, E. P.; Fernandez-Trillo, F.; Alexander, C.; Padgett, M. J.; Cronin, L. *Angew. Chem., Int. Ed.* **2012**, *51*, 12754−12758.
(15) Thouvenel-Romans, S.; van Saarloos, W.; Steinbock, O. *Europhys. Lett.* **2004**, *67*, 42−48.
(16) Makki, R.; Al-Humiari, M.; Dutta, S.; Steinbock, O. *Angew. Chem., Int. Ed.* **2009**, *48*, 8752−8756.
(17) Balköse, D.; Özkan, F.; Köktürk, U.; Ulutan, S.; Ülkü, S.; Nişli, G. *J. Sol-Gel Sci. Technol.* **2002**, *23*, 253−263.
(18) Pagano, J. J.; Thouvenel-Romans, S.; Steinbock, O. *Phys. Chem. Chem. Phys.* **2007**, *9*, 110−118.
(19) McGlynn, S. E.; Kanik, I.; Russell, M. J. *Phil. Trans. R. Soc. A* **2012**, *370*, 3007−3022.
(20) Stone, D. A.; Goldstein, R. E. *Proc. Natl. Acad. Sci. U. S. A.* **2004**, *101*, 11537−11541.
(21) Takiguchi, M.; Igarashi, K.; Azuma, M.; Ooshima, H. *Cryst. Growth Des.* **2006**, *6*, 1611−1614.
(22) Collins, C.; Zhou, W.; Mackay, A. L.; Klinowski, J. *Chem. Phys. Lett.* **1998**, *286*, 583−592.
(23) Ritchie, C.; Cooper, G. J. T.; Song, Y. F.; Streb, C.; Yin, H. B.; Parenty, A. D. C.; MacLaren, D. A.; Cronin, L. *Nat. Chem.* **2009**, *1*, 47−52.
(24) Collins, C.; Mokaya, R.; Klinowski, J. *Phys. Chem. Chem. Phys.* **1999**, *1*, 4669−4672.

Article

(25) Pagano, J. J.; Bánsági, T.; Steinbock, O. *Angew. Chem., Int. Ed.* **2008**, *47*, 9900−9903.

(26) Makki, R.; Steinbock, O. *J. Am. Chem. Soc.* **2012**, *134*, 15519−15527.

(27) Thouvenel-Romans, S.; Steinbock, O. *J. Am. Chem. Soc.* **2003**, *125*, 4338−4341.

(28) Pagano, J. J.; Bánsági, T.; Steinbock, O. *J. Phys. Chem. C* **2007**, *111*, 9324−9329.

(29) Roszol, L.; Steinbock, O. *Phys. Chem. Chem. Phys.* **2011**, *13*, 20100−20103.

(30) Talapin, D. V.; Lee, J. S.; Kovalenko, M. V.; Shevchenko, E. V. *Chem. Rev.* **2010**, *110*, 389−458.

(31) Michalet, X.; Pinaud, F.; Bentolila, L.; Tsay, J.; Doose, S.; Li, J.; Sundaresan, G.; Wu, A.; Gambhir, S.; Weiss, S. *Science* **2005**, *307*, 538−544.

(32) Mattoussi, H.; Palui, G.; Na, H. B. *Adv. Drug Delivery Rev.* **2012**, *64*, 138−166.

(33) Minti, H.; Eyal, M.; Reisfeld, R.; Berkovic, G. *Chem. Phys. Lett.* **1991**, *183*, 277−282.

(34) Norberg, N. S.; Kittilstved, K. R.; Amonette, J. E.; Kukkadapu, R. K.; Schwartz, D. A.; Gamelin, D. R. *J. Am. Chem. Soc.* **2004**, *126*, 9387−9398.

(35) Reda, S. M. *Acta Mater.* **2008**, *56*, 259−264.

(36) Nam, J.; Won, N.; Bang, J.; Jin, H.; Park, J.; Jung, S.; Jung, S.; Park, Y.; Kim, S. *Adv. Drug Delivery Rev.* **2013**, *65*, 622−648.

(37) Zorn, M.; Bae, W. K.; Kwak, J.; Lee, H.; Lee, C.; Zentel, R.; Char, K. *ACS Nano* **2009**, *3*, 1063−1068.

(38) Tvrdy, K.; Frantsuzov, P. A.; Kamat, P. V. *Proc. Natl. Acad. Sci. U. S. A.* **2011**, *108*, 29−34.

(39) Robel, I.; Kuno, M.; Kamat, P. V. *J. Am. Chem. Soc.* **2007**, *129*, 4136−4137.

(40) Reiss, P.; Bleuse, J.; Pron, A. *Nano Lett.* **2002**, *2*, 781−784.

(41) Clapp, A. R.; Goldman, E. R.; Mattoussi, H. *Nat. Protocols* **2006**, *1*, 1258−1267.

(42) Dabbousi, B. O.; Rodriguez-Viejo, J.; Mikulec, F. V.; Heine, J. R.; Mattoussi, H.; Ober, R.; Jensen, K. F.; Bawendi, M. G. *J. Phys. Chem.* **1997**, *101*, 9463−9475.

(43) Mattoussi, H.; Cumming, A. W.; Murray, C. B.; Bawendi, M. G.; Ober, R. *Phys. Rev. B* **1998-II**, *58*, 7850−7863.

(44) Susumu, K.; Uyeda, H. T.; Medintz, I. L.; Pons, T.; Delehanty, J. B.; Mattoussi, H. *J. Am. Chem. Soc.* **2007**, *129*, 13987−13996.

(45) Makki, R.; Steinbock, O. *J. Phys. Chem. C* **2011**, *115*, 17046−17053.

(46) Chen, Y.; Rosenzweig, Z. *Anal. Chem.* **2002**, *74*, 5132.

(47) Xie, H.-Y.; Liang, J.-G.; Zhang, Z.-L.; Liu, Y.; He, Z.-K.; Pang, D. W. *Spectrochim. Acta, Part A* **2004**, *60*, 2527−2530.

(48) Ali, E. M.; Zheng, Y.; Yu, H.-h.; Yang, J. Y. *Anal. Chem.* **2007**, *79*, 9452.

(49) Bähr, G.; Ayalon, A.; Rompf, F. D.; Hirsch-Ayalon, P. *J. Membr. Sci.* **1984**, *20*, 103−111.

(50) Roszol, L.; Makki, R.; Steinbock, O. *Chem. Commun.* **2013**, *49*, 5736−5738.

(51) Noorduin, W. L.; Grinthal, A.; Mahadevan, L.; Aizenberg, J. *Science* **2013**, *340*, 832−837.

(52) Garcia-Ruiz, J. M.; Melero-García, E.; Hyde, S. T. *Science* **2009**, *323*, 362−365.

(53) Kellermeier, M.; Glaab, F.; Melero-García, E.; Garcia-Ruíz, J. M. *Methods Enzymol.* **2013**, *532*, 225−256.

(54) Cartwright, J. H. E.; Escribano, B.; Gonzalez, D. L.; Sainz-Siaz, C. I.; Tuval, I. *Langmuir* **2013**, *29*, 7655−7660.

(55) Corliss, J. B.; Dymond, J.; Gordon, L. I.; Edmond, J. M.; von Herzen, R. P.; Ballard, R. D.; Green, K.; Williams, D.; Bainsbridge, A.; Crane, K.; van Andel, T. H. *Science* **1979**, *203*, 1073−1083.

(56) Double, D. D.; Hellawell, A. *Nature* **1976**, *261*, 486−488.